Eleventh International Conference on CFD in the Minerals and Process Industries
CSIRO, Melbourne, Australia
7-9 December 2015

SIMULATION OF FLOW OF FIBRE SUSPENSIONS USING AN IRBF-BCF BASED MULTISCALE APPROACH

H.Q. NGUYEN[1*], **C.-D. TRAN**[1], **T. TRAN-CONG**[1]

[1]Computational Engineering and Science Research Centre, Faculty of Health, Engineering and Science, The University of Southern Queensland, Toowoomba, QLD 4350, AUSTRALIA

[*] Corresponding author, E-mail address: hung.nguyen@usq.edu.au

ABSTRACT

In this paper, a multiscale method based on the combination of the Integrated Radial Basis Function (IRBF) approximation and the Brownian Configuration Field (BCF) approach is used to simulate the mechanical behaviours of flow of fibre suspensions. The bulk properties of flow including velocity and stresses are governed by conservation equations in continuum mechanics. Meanwhile the evolution of fibres' configuration such as the position and direction of fibres are described by the Jeffery's motion equation in the Eulerian form. The decoupled calculations at two different scales are linked together through the formula of stress by Lipscomb, by which the mutual influence between the kinematic properties of flow and the dynamic behaviours of fibres is represented. In this work, the IRBF based approximations are employed in two separate processes of the numerical discretisation. While the IRBF high-order approximations yield higher accuracy and faster convergence of the method, they might enhance the stability of the fibre dynamics simulation as well, especially for the case of concentrated fibre suspension. The validity of the method is demonstrated by simulating flows of different fibre concentrations between two parallel plates.

Keywords: Multiscale method, Brownian Configuration Field, Integrated Radial Basis Function, dilute fibre suspension flow.

NOMENCLATURE

a_r	fibre's aspect ratio.
$\mathbf{D}$	rate of strain tensor.
k_f	fibre parameter.
n_p	number of collocation points.
N_f	number of fibre configuration fields.
p	dimensionless pressure.
$\mathbf{P}$	direction unit vector of fibre.
$\mathbf{Q}$	length vector of fibre.
Re	Reynold number.
t	dimensionless time.
$\mathbf{u}$	dimensionless velocity vector.
u, v	two components on x and y directions of $\mathbf{u}$.
ϕ	volume fraction of fibre.
η_0	Newtonian fluid viscosity, $[kg/ms]$
λ	dependent parameter of a_r.
μ	material constant, $[kg/ms]$.
θ	angle between the x-axis and the fibre's axis.
$\boldsymbol{\tau}_e$	extra-stress tensor.
$\boldsymbol{\tau}_f$	fibre-contributed stress tensor.
$\boldsymbol{\tau}_s$	solvent-contributed stress tensor.
ω	vorticity.
$\boldsymbol{\Omega}$	vorticity tensor.
Ψ	stream function.

INTRODUCTION

Fibre-reinforced composite materials, e.g. polymer matrices strengthened by glass fibres, are popularly used in many important industrial areas because of their advanced mechanical properties such as high strength and stiffness but low density. These exceptional properties are mostly dominated by the position and direction of fibres existing inside surrounding matrices. Hence, a competent understanding of the orientation distribution of fibre configurations in the solvent is very important and needs to be carefully investigated by researchers in both experimental and numerical aspects.

From the literature, a numerical simulation of fibre suspension basically consists of three following steps (Chiba *et al.*, 2001). In the first step, a fibre stress term is added to the momentum conservation equation to include dynamic effects of fibre on the bulk properties of the flow. The second step is to use an equation of motion to describe the evolution of fibres, where the Jeffery's equation is suitable for dilute suspension while the Folgar and Tucker's equation is applicable for semi-dilute and concentrated ones. The final step is to use a model to calculate the fibre stress from fibre configurations.

The fibre stress tensor is determined by the fourth-order orientation tensor $\langle \mathbf{PPPP} \rangle$. There are two main approaches used to calculate the $\langle \mathbf{PPPP} \rangle$ tensor. One method relies on a closure approximation such as the quadratic or orthotropic ones (Advani *et al.*, 1987; Cintra Jr and Tucker III, 1995) and the other method is based on the idea of Brownian Configuration Field (BCF) developed by Hulsen *et al.* (1997). Whereas the closure approximation approach has shown several non-physical behaviours and the uncertainty in the solution (Szeri and Leal, 1994), the BCF has emerged as a robust method for the simulation of fibre suspensions in complex flows (Fan *et al.*, 1999; Lu *et al.*, 2006; Dou *et al.*, 2007). For this approach, a large number of fibre configuration fields is generated on each and every computational nodes and the fourth-order tensors are then averagely calculated. This yields a good convergent solution, even at high levels of concentration of fibre (Fan *et al.*, 1999).

Recently, the IRBF-BCF macro-micro multiscale approach was derived to successfully simulate a range of polymer solutions (Tran *et al.*, 2011, 2012; Nguyen *et al.*, 2015). Owing to the advantages of the IRBF-based numerical scheme (Mai-Duy and Tran-Cong, 2001), the method possesses the high accuracy solution and the fast numerical convergence. In this paper, one-dimensional IRBF (1D-IRBF) scheme (Mai-Duy and Tran-Cong, 2007) is employed to solve the vorticity-stream function based conservation equations, whereas the fibre configuration governed by the Jeffery's equation is approximated using BCF approach to determine the fibre stress tensor with the Lipscomb's model. The combination of IRBF-based approximations and the BCF technique is expected to enhance the stability and the

accuracy of the solution.

THE GOVERNING EQUATIONS FOR FIBRE SUSPENSION FLOW IN DIMENSIONLESS FORM

Consider an isothermal and incompressible flow of fibre suspensions in two-dimensional (2-D) space. The continuity and momentum equations for the flow in dimensionless form are given by (Lu *et al.*, 2006)

$$\nabla \cdot \mathbf{u} = 0, \tag{1}$$

$$\frac{\partial \mathbf{u}}{\partial t} + \mathbf{u} \cdot \nabla \mathbf{u} = -\nabla p + \frac{1}{Re} \nabla \cdot \boldsymbol{\tau}_e, \tag{2}$$

where t, $\mathbf{u}$, p and $\boldsymbol{\tau}_e$ are the time, velocity field, pressure and extra-stress tensor in the dimensionless form, respectively and Re the Reynolds number. For fibre suspensions in a Newtonian solvent, the extra-stress tensor ($\boldsymbol{\tau}_e$) consists of two components as follows.

$$\boldsymbol{\tau}_e = \boldsymbol{\tau}_s + \boldsymbol{\tau}_f, \tag{3}$$

where $\boldsymbol{\tau}_s = 2\mathbf{D}$ and $\boldsymbol{\tau}_f$ are stress components contributed by Newtonian solvent and fibre suspensions, respectively and $\mathbf{D} = \frac{1}{2}\left(\nabla \mathbf{u} + (\nabla \mathbf{u})^{\mathbf{T}}\right)$ the rate of strain tensor.

There are several models used to calculate the stress contributed by fibre suspensions, for example, the Lipscomb model (Lipscomb *et al.*, 1988) for dilute suspensions and Phan-Thien and Graham model (Phan-Thien and Graham, 1991) for semi-dilute and concentrated suspensions. In this paper, the former one is used to investigate the present method in the simulation of the flow of dilute fibre suspensions. The Lipscomb model is given by

$$\boldsymbol{\tau}_f = k_f \mathbf{D} : \langle \mathbf{PPPP} \rangle, \tag{4}$$

where η_0 is the Newtonian fluid viscosity; $\mathbf{P}$ the orientation unit vector of fibre; $\langle(\cdot)\rangle$ the statistical average of $(\cdot)$ and $\langle \mathbf{PPPP} \rangle$ the fourth order orientation tensor or structure tensor. The dimensionless quantity k_f is the fibre parameter and written by

$$k_f = \frac{\phi \mu}{\eta_0}, \tag{5}$$

where ϕ is the volume fraction of fibres and defined as the volume of all fibres in one unit volume of the flow; and μ is the material constant, which is chosen in the limit of a high aspect ratio of fibre as follows (Chiba *et al.*, 2001).

$$\mu = \frac{\eta_0 {a_r}^2}{\ln(a_r)}, \tag{6}$$

where a_r is the aspect ratio of the fibre.

Substituting Eq. (6) into Eq. (5) yields $k_f = \frac{\phi {a_r}^2}{\ln(a_r)}$. Therefore, the fibre parameter is considered as the single one in the fibre stress equation (4), which describes the impact of fibre suspension on the kinematic behaviour of the flow.

The evolution of fibres' orientation in flow is captured by the Jeffery's equation as (Lipscomb *et al.*, 1988)

$$\frac{\partial \mathbf{P}}{\partial t} + \mathbf{u} \cdot \nabla \mathbf{P} = \boldsymbol{\Omega} \cdot \mathbf{P} + \lambda \left(\mathbf{D} - \mathbf{D} : \mathbf{PPI}\right) \cdot \mathbf{P}, \tag{7}$$

where $\boldsymbol{\Omega} = \frac{1}{2}\left((\nabla \mathbf{u})^T - \nabla \mathbf{u}\right)$ is the vorticity tensor; λ a dependent parameter of aspect ratio, $\lambda = \frac{a_r^2 - 1}{a_r^2 + 1}$ and $\mathbf{I}$ the identity matrix. Like in (Chiba *et al.*, 2001), the parameter λ is chosen as 1 in this paper.

It is worth noting in Eq. (7) that the orientation unit vector $\mathbf{P}$ is a function of space and time ($\mathbf{P} = \mathbf{P}(\mathbf{x}, t)$). However, its unit length ($\|\mathbf{P}\|$) is often violated by numerical simulations due to computational errors. Therefore, a configuration field $\mathbf{Q}(\mathbf{x}, t)$, which is no concern of fibre's length, is introduced as follows.

$$\mathbf{Q}(\mathbf{x}, t) = Q\mathbf{P}(\mathbf{x}, t), \tag{8}$$

where Q is the modulus of $\mathbf{Q}$. With $\lambda = 1$, the Jeffrey' equation (7) is rewritten for the evolution of $\mathbf{Q}$ as follows.

$$\frac{\partial \mathbf{Q}}{\partial t} + \mathbf{u} \cdot \nabla \mathbf{Q} = (\nabla \mathbf{u})^T \cdot \mathbf{Q}. \tag{9}$$

The fourth order orientation tensor $\langle \mathbf{PPPP} \rangle$ can be now defined by

$$\langle \mathbf{P}_i \mathbf{P}_i \mathbf{P}_i \mathbf{P}_i \rangle = \frac{1}{N_f} \sum_{i=1}^{N_f} \left\langle \frac{\mathbf{Q}_i}{Q_i} \frac{\mathbf{Q}_i}{Q_i} \frac{\mathbf{Q}_i}{Q_i} \frac{\mathbf{Q}_i}{Q_i} \right\rangle, \tag{10}$$

where N_f is the number of fibres. The components of the tensor $\langle \mathbf{PPPP} \rangle$ in a two-dimensional fibre orientation field are given by (Chiba *et al.*, 2001)

$$\begin{aligned} P_{1111} &= \sum_{i=1}^{N_f} \frac{\cos^4 \theta_i}{N_f}, \quad P_{1112} = \sum_{i=1}^{N_f} \frac{\cos^3 \theta_i \sin \theta_i}{N_f}, \\ P_{1122} &= \sum_{i=1}^{N_f} \frac{\cos^2 \theta_i \sin^2 \theta_i}{N_f}, \quad P_{1222} = \sum_{i=1}^{N_f} \frac{\cos \theta_i \sin^3 \theta_i}{N_f}, \\ P_{2222} &= \sum_{i=1}^{N_f} \frac{\sin^4 \theta_i}{N_f}, \end{aligned} \tag{11}$$

where θ_i is the angle between the x-axis and the axis of fibre i.

The quantities P_{1111} and P_{1122} are also given by $P_{1111} = \langle P_1 P_1 P_1 P_1 \rangle$ and $P_{1122} = \langle P_1 P_1 P_2 P_2 \rangle$, where P_1 and P_2 are two components of the unit vector $\mathbf{P}$ along x-direction and y-direction, respectively.

A VORTICITY-STREAM FUNCTION FORMULATION FOR SIMULATIONS OF FIBRE SUSPENSION FLOW

In this paper, the vorticity-stream function approach is used to solve the macroscopic governing equations (1) and (2). Let x and y be two orthogonal coordinates of a 2-D space and x is chosen as the flow direction; u and v are two velocity components along x and y directions, respectively. The velocity-vorticity and velocity-stream function relations are given by

$$\omega = \frac{1}{2}\left(\frac{\partial u}{\partial y} - \frac{\partial v}{\partial x}\right), \tag{12}$$

$$u = \frac{\partial \Psi}{\partial y}, \quad v = -\frac{\partial \Psi}{\partial x}, \tag{13}$$

where ω and Ψ are vorticity and stream function variables, respectively.

Taking the curl of Eq. (2) and using Eqs. (1), (3) and (12), the vorticity transport equation of fibre suspension flow is expressed as

$$\begin{aligned} \frac{\partial \omega}{\partial t} + u\frac{\partial \omega}{\partial x} + v\frac{\partial \omega}{\partial y} &= \frac{1}{Re}\left(\frac{\partial^2 \omega}{\partial x^2} + \frac{\partial^2 \omega}{\partial y^2}\right) \\ &+ \frac{1}{2Re}\left(\frac{\partial^2 \tau_f^{xx}}{\partial x \partial y} + \frac{\partial^2 \tau_f^{xy}}{\partial y^2} - \frac{\partial^2 \tau_f^{yx}}{\partial x^2} - \frac{\partial^2 \tau_f^{yy}}{\partial x \partial y}\right), \end{aligned} \tag{14}$$

where τ_f^{xx}, τ_f^{xy}, τ_f^{yx} and τ_f^{yy} are the stress components of the symmetric fibre stress tensor $\boldsymbol{\tau}_f$.
Substituting expressions in Eq. (13) into Eq. (12) yields the equation for stream function as follows.

$$\frac{\partial^2\Psi}{\partial x^2}+\frac{\partial^2\Psi}{\partial y^2}=2\omega. \tag{15}$$

NUMERICAL METHOD

In this work, an IRBF-BCF multiscale approach is used to simulate fibre suspension flows where a semi-implicit scheme is applied to discretise both the vorticity equation (14) and the equation of fibre configuration fields (9) with respect to time. At each time step, the 1D-IRBF scheme is employed to approximate both the field variables of flow and the fibre configuration field.

The 1D-IRBF based spatial discretisation scheme

Consider a second order one-dimensional elliptic differential equation of a variable $\omega=\omega(x)$ and its boundary conditions as follows.

$$\mathscr{L}\omega=f \quad (x\in\Gamma), \qquad \mathscr{B}\omega=h \quad (x\in\partial\Gamma), \tag{16}$$

where $\mathscr{L}$ is the second order differential operator; $\mathscr{B}$ the operator expressing the boundary conditions; f and h the known functions; and Γ and $\partial\Gamma$ the domain and boundary of the variable ω.
For IRBF-based methods, the highest order derivative (the second order one in this case), the lower order derivatives and the original function are decomposed by a set of RBFs and their RBF weights as follows (Mai-Duy and Tran-Cong, 2007).

$$\frac{d^2\omega}{dx^2}=\sum_{j=1}^{m}w_j(t)\,g_j(x)=\sum_{j=1}^{m}w_j(t)\,G_j^{[2]}(x), \tag{17}$$

$$\frac{d\omega}{dx}=\sum_{j=1}^{m}w_j(t)\,G_j^{[1]}(x)+C_1(t), \tag{18}$$

$$\omega(x,t)=\sum_{j=1}^{m}w_j(t)\,G_j^{[0]}(x)+C_1(t)\,x+C_2(t), \tag{19}$$

where $\left\{w_j(t)\right\}_{j=1}^{m}$ is the RBF weights, m the number of grid lines; $\left\{g_j(x)\right\}_{j=1}^{m}$ is the RBFs; $G_j^{[1]}(x)=\int G_j^{[2]}(x)\,dx$; $G_j^{[0]}(x)=\int G_j^{[1]}(x)\,dx$; and C_1 and C_2 unknown integration constants. In this paper, the multi-quadric RBFs (MQ-RBFs) is used and given by

$$g_j(x)=\sqrt{(x-c_j)^2+a_j^2}, \tag{20}$$

where $\left\{c_j\right\}_{j=1}^{m}$ and $\left\{a_j\right\}_{j=1}^{m}$ are RBF centres and widths, respectively. A set of collocation points $\left\{x_j\right\}_{j=1}^{m}$ is taken to be the set of centres.
The Eqs. (17), (18) and (19) are written on every collocation point and re-arranged to produce the following set of algebraic equations

$$\widehat{\frac{d^2\boldsymbol{\omega}}{dx^2}}=\widehat{\mathbf{G}}^{[2]}\widehat{\mathbf{w}}, \qquad \widehat{\frac{d\boldsymbol{\omega}}{dx}}=\widehat{\mathbf{G}}^{[1]}\widehat{\mathbf{w}}, \qquad \widehat{\boldsymbol{\omega}}=\widehat{\mathbf{G}}^{[0]}\widehat{\mathbf{w}}, \tag{21}$$

where

$$\widehat{\mathbf{w}}=\begin{pmatrix} w_1(t) & w_2(t) & \cdots & w_m(t) & C_1(t) & C_2(t)\end{pmatrix}^T;$$

$$\widehat{\boldsymbol{\omega}}=\begin{pmatrix} \omega_1(t) & \omega_2(t) & \cdots & \omega_m(t)\end{pmatrix}^T \text{ with } \omega_j=\omega(x_j);$$

$$\widehat{\frac{d^i\boldsymbol{\omega}}{dx^i}}=\begin{pmatrix} \frac{d^i\omega_1(x,t)}{dx^i} & \frac{d^i\omega_2(x,t)}{dx^i} & \cdots & \frac{d^i\omega_m(x,t)}{dx^i}\end{pmatrix}^T;$$

$$\widehat{\mathbf{G}}^{[i]}=\begin{bmatrix} G_1^{[i]}(x_1) & \cdots & G_m^{[i]}(x_1) & a_1^{[i]} & b_1^{[i]} \\ \vdots & \ddots & \vdots & \vdots & \vdots \\ G_1^{[i]}(x_m) & \cdots & G_m^{[i]}(x_m) & a_m^{[i]} & b_m^{[i]}\end{bmatrix},$$

with $i=\{0,1,2\}$ and

$$\left(a_1^{[i]},a_2^{[i]},\ldots,a_m^{[i]}\right)^T=\begin{cases}(0\ \cdots\ 0)^T, i=2\\ (1\ \cdots\ 1)^T, i=1\\ (x_1\ \cdots\ x_m)^T, i=0\end{cases};$$

$$\left(b_1^{[i]},b_2^{[i]},\ldots,b_m^{[i]}\right)^T=\begin{cases}(0\ \cdots\ 0)^T, i=1,2\\ (1\ \cdots\ 1)^T, i=0\end{cases}.$$

Owing to the presence of integration constants in the IRBF based approximation, more additional constraints can be incorporated into the algebraic equation system through the last equation of (21) as follows.

$$\begin{pmatrix}\widehat{\boldsymbol{\omega}}\\ \widehat{\mathbf{f}}\end{pmatrix}=\widehat{\mathbf{C}}\widehat{\mathbf{w}},$$

where $\widehat{\mathbf{C}}=\begin{bmatrix}\widehat{\mathbf{G}^{[0]}}\\ \widehat{\mathbf{L}}\end{bmatrix}$ and $\widehat{\mathbf{f}}=\widehat{\mathbf{L}}\widehat{\mathbf{w}}$ are additional constraints.
It is preferable to be working with variables in the physical space, so a transformation is done as follows.

$$\widehat{\mathbf{w}}=\widehat{\mathbf{C}}^{-1}\begin{pmatrix}\widehat{\boldsymbol{\omega}}\\ \widehat{\mathbf{f}}\end{pmatrix}, \tag{22}$$

where $\widehat{\mathbf{C}}^{-1}$ is the conversion matrix. Eq. (22) is substituted into Eqs. (17) and (18) to obtain the second and first-order derivatives of ω in terms of nodal variable values as

$$\frac{d^2\omega}{dx^2}=\mathscr{D}_2\widehat{\boldsymbol{\omega}}+k_2, \qquad \frac{d\omega}{dx}=\mathscr{D}_1\widehat{\boldsymbol{\omega}}+k_1 \tag{23}$$

where $\mathscr{D}_1$ and $\mathscr{D}_2$ are known vectors of length m; and k_2 and k_1 are scalars determined by $\widehat{\mathbf{f}}$. Applying Eq. (23) at every collocation points yields

$$\widehat{\frac{d^2\boldsymbol{\omega}}{dx^2}}=\widehat{\mathscr{D}}_{2x}\widehat{\boldsymbol{\omega}}+\widehat{\mathbf{k}}_{2x}, \qquad \widehat{\frac{d\boldsymbol{\omega}}{dx}}=\widehat{\mathscr{D}}_{1x}\widehat{\boldsymbol{\omega}}+\widehat{\mathbf{k}}_{1x} \tag{24}$$

where $\widehat{\mathscr{D}}_{2x}$ and $\widehat{\mathscr{D}}_{1x}$ are known matrices of dimension $m\times m$; $\widehat{\mathbf{k}}_{2x}$ and $\widehat{\mathbf{k}}_{1x}$ are known vectors of length m and m is defined as before. The subscript x expresses the spatial direction, on which the matrices ($\widehat{\mathscr{D}}_{2x}$, $\widehat{\mathscr{D}}_{1x}$) and the vectors ($\widehat{\mathbf{k}}_{2x}$, $\widehat{\mathbf{k}}_{1x}$) are constructed. For 2-D problems, a similar process is proceeded on y-direction in order to achieve known matrices and vectors $\widehat{\mathscr{D}}_{2y}$, $\widehat{\mathscr{D}}_{1y}$, $\widehat{\mathbf{k}}_{2y}$ and $\widehat{\mathbf{k}}_{1y}$. After obtaining these known matrices and vectors, equations (14) and (8) can be solved with appropriate boundary conditions at each time step.

Time discretisation of the vorticity transport equation and the equation of fibre configuration fields

In order to temporally discretise the vorticity transport equation (14), the Crank-Nicolson scheme is used for the diffusion term while the Euler explicit scheme is for the convection term. The resultant discrete equation is given by

$$\omega^{n+1} - \frac{\Delta t}{2Re}\left(\frac{\partial^2\omega^{n+1}}{\partial x^2} + \frac{\partial^2\omega^{n+1}}{\partial y^2}\right) = \omega^n + \frac{\Delta t}{2Re}\left(\frac{\partial^2\omega^n}{\partial x^2} + \frac{\partial^2\omega^n}{\partial y^2}\right) - \Delta t u^n\frac{\partial\omega^n}{\partial x} - \Delta t v^n\frac{\partial\omega^n}{\partial y} + \frac{\Delta t}{2Re}\left(\frac{\partial^2(\tau_f^{xx})^n}{\partial x\partial y} + \frac{\partial^2(\tau_f^{xy})^n}{\partial y^2} - \frac{\partial^2(\tau_f^{yx})^n}{\partial x^2} - \frac{\partial^2(\tau_f^{yy})^n}{\partial x\partial y}\right), \tag{25}$$

where superscripts $(n+1)$ and n indicates the two successive time steps at $t_{n+1} = (n+1)\Delta t$ and $t_n = n\Delta t$, respectively. The components of fibre stress tensor τ_f^{xx}, τ_f^{xy}, τ_f^{yx} and τ_f^{yy} are known quantities, which are calculated from the fibre configuration fields.

The temporal discretisation of the equation of fibre configuration fields Eq. (8) is carried out using the Crank-Nicolson scheme as follows.

$$\mathbf{Q}(\mathbf{x},t_{n+1}) + \frac{\Delta t}{2}\mathbf{u}(\mathbf{x},t_n)\cdot\nabla\mathbf{Q}(\mathbf{x},t_{n+1}) = \mathbf{Q}(\mathbf{x},t_n) - \frac{\Delta t}{2}\mathbf{u}(\mathbf{x},t_n)\cdot\nabla\mathbf{Q}(\mathbf{x},t_n) + \Delta t\left(\nabla\mathbf{u}(\mathbf{x},\mathbf{t_n})\right)^T\cdot\mathbf{Q}(\mathbf{x},t_n), \tag{26}$$

where $t_n = n\Delta t$ and $t_{n+1} = (n+1)\Delta t$ are time at steps n and $(n+1)$, respectively; and Δt the time step size.

It is worth noting that the velocity field and its gradient in Eq. (26) are known and obtained by the numerical approximation of vorticity-stream functions. For the stability of the present method, high-order upwind schemes (Ferreira *et al.*, 2002) are applied to approximate the gradient of the fibre configuration field ($\nabla\mathbf{Q}$) at the right-hand-side of Eq. (26).

Since the fibre configuration fields, $\mathbf{Q}_i$, $i = (1,2,\cdots,N_f)$, are independent with each other, (26) can be processed in parallel. The configuration fields of $\mathbf{Q}_i$'s are then conversed to the orientation unit vector of fibres $\mathbf{P}_i$'s using Eq. (8) for the solutions of the fourth-order orientation tensor and the fibre stress. Thus, the fibre stress is known in the transport vorticity equation (14).

A NUMERICAL EXAMPLE

In this section, a flow of fibre suspensions between two parallel plates is simulated using the present method. This problem was previously studied by Chiba *et al.* (2001) using a combined approach based on the finite different method and a statistical simulation for fibre configurations.

The geometry of the problem is given as in Fig. 1, where $L = 10$ and $H = 1$ are the length and height of the channel, respectively. The Lipscomb's fibre stress model is used with a range of values of fibre parameter, $k_f = \{2,6,10\}$. The other parameters used in the simulation include: the Reynold number, $Re = 10$; the time step size, $\Delta t = 0.001$; and the number of fibre configuration fields, $N_f = 180$.

Cartesian grid and boundary conditions

Let Δx and Δy be grid spaces on x and y-directions, respectively. A non-uniform Cartesian grid described in Fig. 2 is used to simulate the problem. The grid's parameters are as follows: $\Delta y = 0.05$ on y-direction; Δx is non-uniform on x-direction with $\Delta x_1 = 0.05$ at regions near the inlet and outlet boundaries and $\Delta x_2 = 0.125$ at the intermediate section of the channel. The numerical experience shows that a finer mesh at regions near the inlet and outlet allows the physical

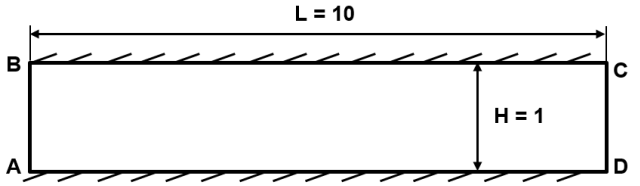

Figure 1: Flow of fibre suspensions between two parallel plates: the geometry of the problem.

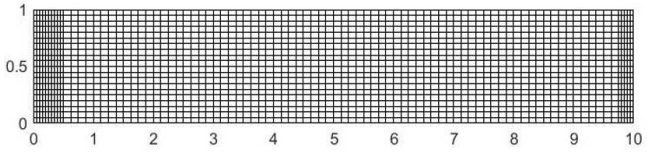

Figure 2: Flow of fibre suspensions between two parallel plates: the non-uniform Cartesian grid is used in the simulation.

behaviours of flow and fibre configurations to be captured accurately in these regions. It is worth noting that a finer mesh of $\Delta x = \Delta y = 0.025$ was used in Chiba *et al.* (2001).

The boundary conditions:

- At the inlet $\overline{AB}$:

  With the velocity field, the flow is fully developed where the velocity profile for the Newtonian fluid in this work is parabolic: $u = u_{max}\left(1 - \left(\frac{2y}{H} - 1\right)^2\right)$ and $v = 0$ where u_{max} is the maximum velocity on the flow direction and chosen as 1.5.

  With the fibre configuration field, a set of N_f fibres is generated and assigned at each collocation point on the inlet boundary. A fibre i is defined by the angle $\theta_i = -\frac{\pi}{2} + \frac{\pi(i-1)}{N_f}$, $(i = 1,...,N_f)$;

- On the walls $\overline{BC}$ and $\overline{AD}$:

  With the velocity field, there is no slip, i.e. $u = 0$ and $v = 0$.

  With the fibre configuration field, co-linear alignment, i.e. $\theta_i = 0$;

- At the outlet $\overline{DC}$:

  A flow out condition is used, i.e. $\frac{\partial u}{\partial x} = 0$ and $v = 0$.

Making use of the approximation schemes presented above, the simulation is terminated when the convergence of field variable(s) is/are reached a preset tolerance as follows.

$$CM(\mathbf{var}) = \sqrt{\frac{\sum_1^{n_p}\sum_{i=1}^{d_s}\left(var_i^n - var_i^{n-1}\right)^2}{\sum_1^{n_p}\sum_{i=1}^{d_s}(var_i^n)^2}} \leq tol, \tag{27}$$

where d_s is the number of dimensions; tol a preset tolerance; var_i the i-component of the field variable **var** at a collocation point; n_p the total number of collocation points; and n the iteration number.

Results and discussion

It can be seen that the present method outperforms the method by Chiba *et al.* (2001) regarding convergence (see Fig. 3). Indeed, for the fibre parameter $k_f = 10$, after 7000 iterations of the simulation, the *CM*s of vorticity, velocity and stream function can reach to 10^{-4}, 10^{-5} and 10^{-6}, respectively whereas they were 10^{-3} and 10^{-4} for the vorticity and the stream function, respectively in Chiba *et al.* (2001) using a finer mesh as mentioned above.

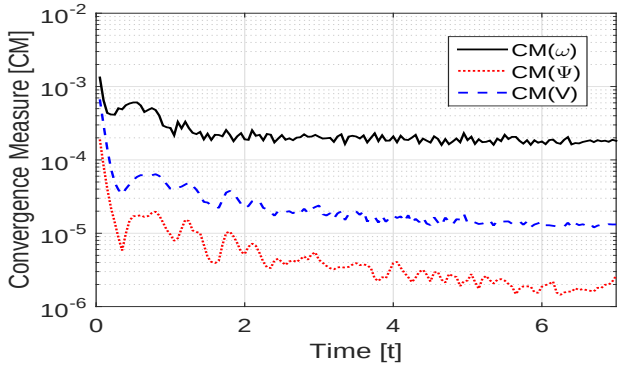

Figure 3: Flow of fibre suspensions between two parallel plates: the convergence measure of velocity, vorticity and stream function with $k_f = 10$.

Fig. 4 describes the development of velocity along the centreline of channel for a range of fibre parameters $k_f = (2,6,10)$. The velocity undershoot is observed for all cases of fibre parameter and reflects the effect of the fibre configuration at the inlet. In other words, a random distribution of fibres' orientation at the inlet resists the development of velocity near the inlet area. The effect of inlet fibre configuration is gradually reduced down-to the outlet and the flow can reach a fully developed state with an enough long channel. Furthermore, the undershoot increases with the increment of fibre parameter.

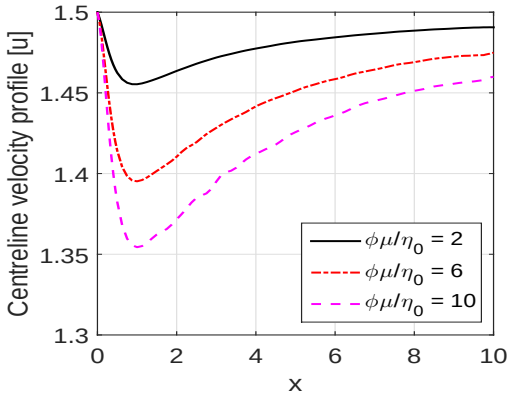

Figure 4: Flow of fibre suspensions between two parallel plates: the centreline velocity profiles with $k_f = (2,6,10)$.

The effect of the fibre parameter on the outlet velocity profiles was also studied and presented in Fig. 5 for a range of $k_f = (2,6,10)$. Results depict the outlet velocity profile of flow become more plug-like with higher values of the fibre parameter as compared with the fully developed outlet velocity profile in the Newtonian fluid.
Figs. 6 describes the distribution of two components P_{1111} (Top figure) and P_{1122} (Bottom figure) of the fourth-order

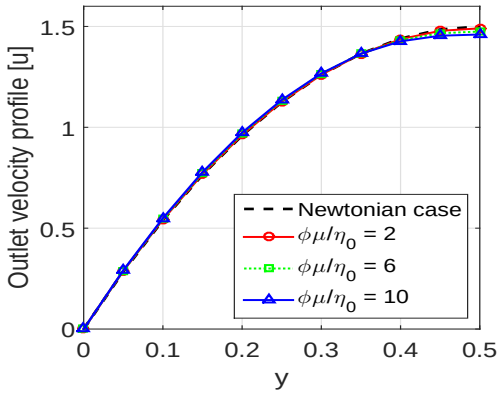

Figure 5: Flow of fibre suspensions between two parallel plates: the velocity profile at the outlet of the Newtonian fluid flow and the fibre suspension flows with $k_f = (2,6,10)$.

tensor $\langle \mathbf{PPPP} \rangle$ on the width of the channel as well as along the channel. The distribution shows that fibres have a tendency to be associated to the flow direction (x-direction in this example) when approaching the outlet. In other words, the components P_{1111} and P_{1122} of tensor $\mathbf{P}$ converge to unity and zero, respectively at the region near the outlet. Furthermore, the isotropic state of fibre configurations is mostly maintained on the centreline along the channel.

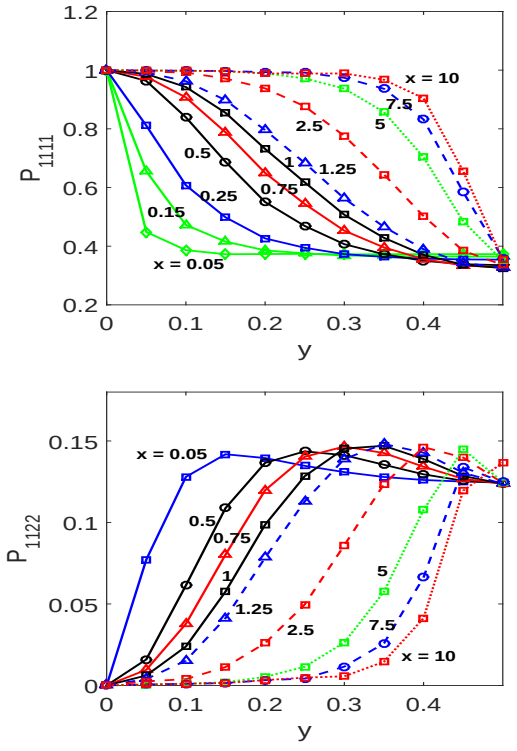

Figure 6: Flow of fibre suspensions between two parallel plates: the distribution of the components P_{1111} (Top figure) and P_{1122} (Bottom figure) along the channel with $k_f = 10$.

The distribution of the shear stress (T_{xy}) and the first normal stress ($T_{xx} - T_{yy}$) of the flow with the fibre parameter $k_f = 10$ are presented in Fig. 7. Results show that in contrast to the Newtonian fluid flow, a high stress concentration appears at the corner between the inlet boundary and the walls in the simulation of the fibre suspension flow. The distribution of

T_{xy} and $T_{xx} - T_{yy}$ as well as their values are close match with those by Chiba *et al.* (2001).

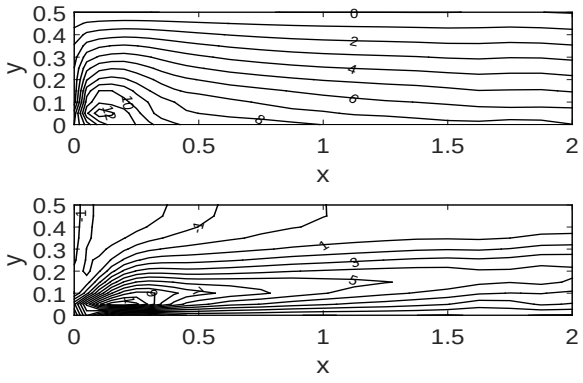

Figure 7: Flow of fibre suspensions between two parallel plates: The distribution of shear stress (Top figure) and the first normal stress difference (Bottom Figure) in flow with $k_f = 10$.

Finally, the orientation of fibres along the channel is described by ellipses whose shape and major axes are determined by the eigenvalues and eigenvectors of the second-order orientation tensor $\langle \mathbf{PP} \rangle$. For example, a circular ellipse implies a fibres' isotropic direction at a collocation point, while a horizontal straight-line ellipse indicates that all fibres at that point completely align with the flow direction. Fig. 8 shows the evolution of the fibres' orientation along the channel. The result shows that the fibres' orientation is strongly impacted by the shear stress field of the flow along the channel (see Fig. 7, Top)and the boundary conditions for fibre configurations at the inlet and the wall. Indeed, the isotropic orientation is maintained at the inlet and the centreline, where having the zero-value shear stress. This isotropic state is gradually reduced to the completely alignment state when approaching the wall, where the maximum shear stress exists.

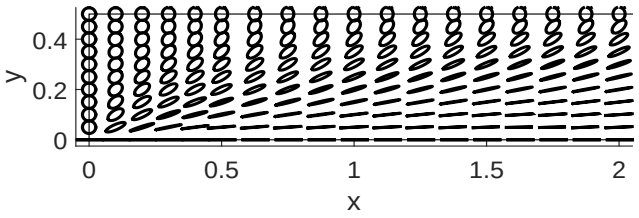

Figure 8: Flow of fibre suspensions between two parallel plates: the evolution of the fibres' orientation from the inlet $x = 0$ to $x = 2$ in flow with $k_f = 10$.

CONCLUSION

This paper reports the use of a 1D-IRBF-BCF method to simulate dilute fibre suspension flows. At a time step, all governing differential equations including the vorticity transport equation and the Jeffery's equation of fibre configuration fields are separately solved using the 1D-IRBF method. The evolution of fibre configurations captured by the Jeffery's equation is approximated using the BCF idea. The two processes are closed by Lipscomb's model. The significant contribution of this work is to integrate the 1D-IRBF scheme into the numerical approximation of two phases solvent and fibres. Taking the advantages of the method, the stability and the accuracy of solutions are significantly improved. Indeed, the obtained results by simulating the fibre suspension flow through a channel including velocity, stress and the distribution of fibre configuration are in very good agreement with those of Chiba *et al.* (2001) whereas the convergence measure is significantly improved even with a coarser mesh used.

ACKNOWLEDGEMENT: The first author would like to thank USQ for a Postgraduate Research scholarship and Scholarship Supplements by FoHES and CESRC. These supports are gratefully acknowledged.

REFERENCES

ADVANI, S. *et al.* (1987). "The use of tensors to describe and predict fiber orientation in short fiber composites". *Journal of Rheology (1978-present)*, **31(8)**, 751–784.

CHIBA, K. *et al.* (2001). "Numerical solution of fiber suspension flow through a parallel plate channel by coupling flow field with fiber orientation distribution". *Journal of non-newtonian fluid mechanics*, **99(2)**, 145–157.

CINTRA JR, J.S. and TUCKER III, C.L. (1995). "Orthotropic closure approximations for flow-induced fiber orientation". *Journal of Rheology (1978-present)*, **39(6)**, 1095–1122.

DOU, H.S. *et al.* (2007). "Simulations of fibre orientation in dilute suspensions with front moving in the filling process of a rectangular channel using level-set method". *Rheologica acta*, **46(4)**, 427–447.

FAN, X.J. *et al.* (1999). "Simulation of fibre suspension flows by the brownian configuration field method". *Journal of non-newtonian fluid mechanics*, **84(2)**, 257–274.

FERREIRA, V.G. *et al.* (2002). "High-order upwinding and the hydraulic jump". *International journal for numerical methods in fluids*, **39(7)**, 549–583.

HULSEN, M.A. *et al.* (1997). "Simulation of viscoelastic flows using brownian configuration fields". *Journal of Non-Newtonian Fluid Mechanics*, **70(1)**, 79–101.

LIPSCOMB, G.G. *et al.* (1988). "The flow of fiber suspensions in complex geometries". *Journal of Non-Newtonian Fluid Mechanics*, **26(3)**, 297–325.

LU, Z. *et al.* (2006). "Numerical simulation of fibre suspension flow through an axisymmetric contraction and expansion passages by brownian configuration field method". *Chemical engineering science*, **61(15)**, 4998–5009.

MAI-DUY, N. and TRAN-CONG, T. (2001). "Numerical solution of differential equations using multiquadric radial basis function networks". *Neural Networks*, **14**, 185–199.

MAI-DUY, N. and TRAN-CONG, T. (2007). "A collocation method based on onedimensional rbf interpolation scheme for solving pdes". *International Journal of Numerical Methods for Heat and Fluid Flow*, **26**, 426–447.

NGUYEN, H.Q. *et al.* (2015). "RBFN stochastic coarse grained simulation method: PartI - Dilute polymer solutions using Bead-Spring Chain models". *CMES: Computer Modeling in Engineering & Sciences*.

PHAN-THIEN, N. and GRAHAM, A.L. (1991). "A new constitutive model for fibre suspensions: flow past a sphere". *Rheologica acta*, **30(1)**, 44–57.

SZERI, A.J. and LEAL, L.G. (1994). "A new computational method for the solution of flow problems of microstructured fluids. part 2. inhomogeneous shear flow of a suspension". *Journal of Fluid Mechanics*, **262**, 171–204.

TRAN, C.D. *et al.* (2011). "An integrated RBFN-based macro-micro multi-scale method for computation of visco-elastic fluid flows". *CMES: Computer Modeling in Engineering and Sciences*, **82(2)**, 137–162.

TRAN, C.D. *et al.* (2012). "A continuum-microscopic method based on IRBFs and control volume scheme for viscoelastic fluid flows". *CMES: Computer Modeling in Engineering and Sciences*, **85(6)**, 499–519.